Ejected-electron-energy and angular dependence of fully differential ionization cross sections in medium-velocity proton collisions with He and H₂

M. Dhital [1], S. Bastola,[1] A. Silvus,[1] J. Davis,[1] B. R. Lamichhane,[1] E. Ali,[2] M. F. Ciappina [3,4]
R. Lomsadze,[5] A. Hasan [6] D. H. Madison,[1] and M. Schulz [1,*]

[1]*Department of Physics and LAMOR, Missouri University of Science & Technology, Rolla, Missouri 65409, USA*
[2]*Department of Natural Sciences, Northwest Missouri State University, Maryville, Missouri 64468, USA*
[3]*ICFO–Institut de Ciencies Fotoniques, The Barcelona Institute of Science and Technology, 08860 Castelldefels, Barcelona, Spain*
[4]*Institute of Physics of the ASCR, ELI Beamlines Project, Na Slovance 2, 18221 Prague, Czech Republic*
[5]*Department of Exact and Natural Science, Tbilisi State University, Tbilisi 0179, Georgia*
[6]*Department of Physics, UAE University, P.O. Box 15551, Al Ain, Abu Dhabi, United Arab Emirates*

We have measured fully momentum-analyzed recoiling target ions and scattered projectiles, produced in ionization of He and H₂ by 75 keV proton impact, in coincidence. The momentum of the ejected electrons was deduced from momentum conservation. From the data we extracted fully differential ionization cross sections as a function of the polar electron emission angle (for fixed electron energies) and as a function of the electron energy (for fixed electron emission angles). Comparison between experiment and various distorted wave calculations confirms that under kinematic conditions where the post-collision interaction plays an important role, the few-body dynamics underlying the ionization process are still poorly understood.

I. INTRODUCTION

One of the most important goals of research in atomic physics is to advance our understanding of the few-body dynamics in simple systems (e.g., [1,2]). Theoretically, this is a problem, which cannot be solved analytically for more than two mutually interacting particles even if the underlying forces are precisely known. Therefore, sophisticated numerical methods need to be developed. The assumptions and approximations entering in these models need to be tested by detailed experimental data. The most sensitive tests of theory are offered by experiments, in which the complete kinematic information of every single particle in the system (kinematically complete experiments) is obtained (for reviews see, e.g., [3–7]).

One process that has attracted particularly strong interest is ionization of simple atoms or molecules by charged particle impact. In the case of electron projectiles, the first kinematically complete experiment was performed already some 50 years ago [8]. Since then, a rich literature on measured fully differential cross sections (FDCS) has emerged covering just about every kinematic configuration conceivable (e.g., [9–19]). Initially, ionization by electron impact was a particularly suitable test case to develop theoretical models. There, the collision system consists of two light particles (the projectile electron and the active target electron) and only one heavy particle (the residual target ion including the passive electrons), where the heavy particle is practically identical with the center of mass of the system. Under such circumstances, the scattered projectiles can be accurately described in terms of just a few angular momentum states, which is a favorable condition for nonperturbative approaches. Indeed, numerous such methods have been developed over the last two decades and good agreement with measured FDCS for ionization of simple targets is routinely achieved (e.g., [2,19–22]).

For ion impact, fully differential studies of ionization, both experimental and theoretical, are much more challenging. Experimentally, the difficulty is that the large projectile mass results in typical scattering angles of only a fraction of a mrad (for fast heavy ions a fraction of a μrad). Furthermore, the projectile energy loss is usually only a tiny fraction of the initial energy, especially for fast heavy ions. As a result, kinematically complete experiments on ionization by ion impact directly momentum analyzing the projectiles (along with the recoil ions) so far have only been performed for 75 keV proton impact (e.g., [7,23–27]). For heavier and faster ions FDCS were measured by momentum analyzing the recoil ions and the ejected electrons in coincidence and deducing the projectile momentum transfer from the kinematic conservation laws (e.g., [1,7,28–35]).

Theoretically, the challenges to nonperturbative approaches also stem from the much larger projectile masses in case of ion-impact compared to electron collisions. As a result, an enormous number of angular momentum states has to be considered to accurately describe the scattered projectiles. Nevertheless, several nonperturbative methods on ionization have been developed in recent years [36–39]. However, comparison of FDCS calculated with these approaches with experimental data is still rather limited and the agreement

---

*schulz@mst.edu

is not as satisfactory as it is for electron impact [37,38]. Research on ion-atom collisions thus still has to rely to a large extent on perturbative models.

One major limitation with the recoil-electron coincidence technique is that fast ejected electrons cannot be measured with sufficiently large effective solid angle. Slow electrons can be confined to the solid angle subtended by the detector by a combination of the electric extraction field and a magnetic field. However, to accomplish this for fast electrons both fields would have to be so large that they would significantly compromise the momentum resolution for both the recoil-ions and the electrons. As a result, FDCS for ionization measured using the recoil-electron coincidence technique so far have only been obtained for electron speeds much smaller than the projectile speed.

Using the scattered projectile-recoil coincidence technique for moderate-energy light-ion impact, it was possible to cover a larger kinematic regime. In the first kinematically complete experiment performed with this method FDCS were obtained for an electron energy around 5 eV [23]. However, later, FDCS were measured for electron speeds close to the projectile speed corresponding to an energy of 40.8 eV, known as the cusp energy (note that in projectile energy loss the cusp energy differs for different targets) [26,27]. For small electron energy the agreement between experiment and perturbative calculations was not very good, but qualitatively satisfactory (e.g., [23,24]). In contrast, near the cusp energy, major discrepancies between experiment and theory were found, especially at large scattering angles [26,27]. Moreover, two conceptually very similar perturbative models did not even qualitatively agree with each other. In this kinematic regime, the collision dynamics are believed to be dominated by a higher-order mechanism known as post-collision interaction (PCI). Apart from the primary interaction lifting the electron to the continuum, it involves a second projectile-electron interaction in the outgoing part of the collision, where they attract each other towards the initial projectile beam axis. The observations of [23,24,26,27] suggest that the kinematic regime around the cusp energy represents a severe limitation to perturbative methods in accurately describing the few-body dynamics. However, so far FDCS were only measured for a few electron energies very close to the cusp energy and for only one energy well below the cusp energy. In between, and at energies well above the cusp energy, fully differential data are lacking. Therefore, systematic conclusions regarding the limitations of perturbative approaches cannot be reached yet.

In this article, we present measured and calculated FDCS for an extended kinematic regime, filling the gap between a very small ejected electron energy and the cusp energy region. The data confirm the severe difficulties of perturbative approaches accurately describing FDCS in the region where PCI is dominant. However, they also demonstrate that, even in regimes where PCI was not expected to be dominant, perturbative approaches do not always lead to accurate results either.

II. EXPERIMENT

The experiment was performed at the medium-energy ion accelerator of the Missouri University of Science and Technology (S&T). Protons were generated with a hot cathode ion source and extracted with an energy of 5 keV. They were then further accelerated to 75 keV by a high-voltage platform. After passing through a pair of collimating slits, the proton beam intersected with very cold target beams (He and H_2) from a supersonic jet ($T = 1–2$ K in the direction of expansion, a fraction of 1 K in the plane perpendicular to the expansion). The collimating slits had a width of 150 μm and were placed at a distance of 50 cm from the target region. This slit geometry corresponds to a transverse coherence length of about 3.3 a.u. [40,41]. This is larger than the internuclear separation in H_2 (1.4 a.u.) and larger than the impact parameter range mostly contributing to ionization. Therefore, the coherence requirement for observable interference is satisfied for molecular two-center as well as for single-center interference [42]. However, it should be noted that a theoretical study demonstrated that even at this relatively large coherence length, the FDCS change very sensitively with the coherence length and the projectiles therefore cannot be regarded as fully coherent [43].

After the collision, the projectiles were charge-state analyzed by a switching magnet. The beam component that did not charge exchange was decelerated by 70 keV, energy analyzed by an electrostatic parallel-plate analyzer [44], and detected by a two-dimensional position sensitive multichannel plate (MCP) detector. The analyzer slits were oriented in the horizontal direction (x direction) and had a width of 75 μm, resulting in an energy resolution of 2.5 eV full width at half maximum (FWHM), and a length of about 2.5 cm. Since the direction of dispersion of the analyzer is in the y direction, the narrow slit width means that only one energy loss (i.e., only one ejected electron energy) could be recorded at a time, i.e., for each energy loss a separate experiment was performed. From the energy, the longitudinal projectile momentum component was determined with a resolution of 0.03 a.u. The x component was obtained from the position information with a resolution of 0.35 a.u. Due to the narrow analyzer slits, the y component was kept fixed at 0 within the resolution of about 0.1 a.u. FWHM.

The recoiling target ions were extracted with a weak electric field of about 6 V/cm in the x direction, momentum analyzed by a COLTRIMS (cold target recoil-ion momentum spectroscopy) apparatus, and detected by another position-sensitive MCP detector. The recoil-ion and projectile detectors were set in coincidence. From the time of flight of the recoil ions from the collision to the detector, contained in the coincidence time, the x component of the recoil momentum was obtained with a resolution of 0.1 a.u. FWHM. The other two components were deduced from the recoil position information. In the z direction, defined by the initial projectile beam direction, the resolution was 0.12 a.u. FWHM. In the y direction, the resolution (0.35 a.u. FWHM) is limited by the temperature of the target gas in the direction of the expansion.

The electron momentum is determined through momentum conservation through the relation $\mathbf{k} = \mathbf{q} - \mathbf{p}_{\text{rec}}$, where $\mathbf{q}$ is the momentum transfer from the projectile to the target and it is the negative of the momentum change vector of the projectile. FDCS were obtained for electrons ejected into the scattering plane spanned by $\mathbf{q}$ and the initial projectile momentum $\mathbf{K}_i$, which in our coordinate system is the xz plane. For fixed projectile scattering angle θ_p the FDCS were analyzed as a function of projectile energy loss ε (or equivalently electron

energy $E_{\text{el}} = \varepsilon - I$, where I is the target ionization potential) for fixed polar electron ejection angles θ_{el} (measured relative to the projectile beam axis) and as a function of θ_{el} for fixed ε. The y component of the electron momentum is only needed to select the scattering plane; however, it does not enter in the determination of θ_{el}. Therefore, the resolution in θ_{el} is nearly unaffected by the resolution in the y components of the measured momenta, which is worse than for the other two components.

In the case of the He target, FDCS were measured for energy losses corresponding to $E_{\text{el}} = \varepsilon - I = 15.4$, 25.4, 32.4, and 35.4 eV, where I is the ionization potential of the ground state of He, and analyzed together with previously published data for $E_{\text{el}} = 5.4$, 37.9, 40.9, 43.9, and 60.4 eV [27]. Here, $E_{\text{el}} = 40.7$ eV corresponds to the cusp energy. For the H_2 target new data were obtained for $E_{\text{el}} = 24.6$ and 54.6 eV in addition to previously published data for $E_{\text{el}} = 14.6$, 34.6, 37.6, 41.6, and 44.6 eV [26]. The FDCS were put on an absolute scale by integrating them over the electron solid angle and normalizing for each energy loss to double differential cross sections in projectile solid angle and electron energy, which were measured previously for He [45] and H_2 [46].

In the case of the He target, ionization plus excitation of the second electron could contribute to the data. The threshold for this process in ε is 65.2 eV so that it cannot contribute to the data for ε up to 62.5 eV ($E_{\text{el}} = 37.9$ eV). Due to the proximity to the threshold, the cross section for ionization excitation at $\varepsilon = 65.5$ eV is entirely negligible compared to single ionization. For the larger energy losses (68.5 and 85 eV or $E_{\text{el}} = 43.9$ and 60.4 eV) the contributions from this process are only significant for θ_p much larger than 0.5 mrad. In the angular range for which we present data here, these contributions do not exceed 5% relative to single ionization and become smaller with decreasing θ_p. In the case of the H_2 target, ionization-excitation results in dissociation of the molecule and thus cannot contribute at all to true coincidences with the recoiling H_2^+ ions.

III. THEORY

Calculations were carried out for He and H_2 using CDW-EIS (continuum distorted-wave eikonal initial-state) and 3DW-EIS (three-body distorted-wave eikonal initial-state) theories as base models. First, we consider ionization of He using the CDW-EIS method. We treat helium single ionization as a single active electron process and assume that in the final state the ejected electron moves in the combined Coulomb field of both the incident ion and the residual target core. Partial screening of the active electron-target interaction due to the "passive" bound helium electron is modeled by effective charges as considered within the usual prior CDW-EIS approach (see below for more details).

In the center-of-mass (CM) frame, fully differential cross sections (FDCS) as a function of the energy and ejection angle of the electron, and direction of the outgoing projectile, can be written as

$$\frac{d^3\sigma}{dE_{\text{el}}d\Omega_{\text{el}}d\Omega_K} = N_e(2\pi)^4\mu^2 k \frac{K_f}{K_i}|T_{fi}|^2\delta(E_f - E_i), \quad (1)$$

where N_e is the number of electrons in the atomic shell, μ is the reduced mass of the projectile-target subsystem, K_i (K_f)

is the magnitude of the initial (final) projectile momentum, and E_i (E_f) is the total initial (final) energy of the system in the CM frame. The ejected electron's energy is given by $E_{\text{el}} = k^2/2$, where k is the magnitude of the electron momentum. The solid angles $d\Omega_K$ and $d\Omega_{\text{el}}$ represent the direction of scattering of the projectile and the ionized electron, respectively. The projectile solid angle $d\Omega_K = \sin\theta_K d\theta_K d\phi_K$ can be expressed in terms of the transversal component magnitude of the momentum transfer $q_\perp$ via the relationship $q_\perp \approx K_i \sin\theta_K \approx K_i\theta_K$ and $K_i \approx K_f$, fulfilled for heavy ions projectiles and small scattering angles. Finally, let us note that the projectile momentum transfer $\mathbf{q} = (\mathbf{q}_\perp, q_z) = \mathbf{K}_i - \mathbf{K}_f$, where $\mathbf{K}_i$ ($\mathbf{K}_f$) is the initial (final) momentum of the incoming particle. In our context $\mathbf{q}_\perp \cdot \widehat{\mathbf{v}} = 0$, where $\widehat{\mathbf{v}}$ is a unit vector that defines the direction of the projectile velocity vector $\mathbf{v}$ and $q_z = \varepsilon/v$.

Let us note that when differential cross sections depend on the projectile scattering angle, for example, the interaction between the projectile and the residual target ion (dubbed PT interaction) may play an important role and is therefore considered in our theoretical analysis. On the other hand, when differential cross sections are functions only of the electron energy and/or angular coordinates, this interaction is not included since their influence in the transition amplitude is reduced to a complex phase factor that gives no contribution to the cross sections values (for details see, e.g., [47,48]). Invoking the eikonal approximation, the PT interaction can be included in the transition amplitude $\mathcal{A}_{if}(\boldsymbol{\rho})$ as a phase factor, which for a pure Coulomb PT interaction yields

$$\mathcal{A}_{if}(\boldsymbol{\rho}) = i(\rho v)^{2iv}\mathcal{A}'_{if}(\boldsymbol{\rho}) \quad (2)$$

with $v = Z_P Z_T/v$, Z_P, and Z_T being the projectile and residual-target ion charges, respectively, and where $\boldsymbol{\rho}$ defines the impact parameter ($\boldsymbol{\rho} \cdot \mathbf{v} = 0$). We consider the PT interaction as a pure Coulomb one between a projectile with charge Z_P and the "bare" target core charge, $Z_T = 1$. Other values for Z_T have been used, to partially account for the screening of the remaining bound electron. However, this choice has little influence on the calculated FDCS. $\mathcal{A}_{if}(\boldsymbol{\rho})$ ($\mathcal{A}'_{if}(\boldsymbol{\rho})$) is the transition amplitude with (without) the PT interaction. Using a two-dimensional Fourier transform it is possible to find a relation between $\mathcal{A}_{if}(\boldsymbol{\rho})$ and $T_{fi}^{(-)}(\mathbf{q}_\perp)$, i.e., the transition matrices as a function of the impact parameter $\boldsymbol{\rho}$ or the transverse component of the momentum transfer $\mathbf{q}_\perp$. Consequently, the transition matrices with and without the PT interaction can be written as

$$T_{fi}'^{(-)}(\mathbf{q}_\perp) = \frac{1}{2\pi}\int d\boldsymbol{\rho}\, e^{i\mathbf{q}_\perp \cdot \boldsymbol{\rho}}\mathcal{A}'_{if}(\boldsymbol{\rho}), \quad (3)$$

$$T_{fi}^{(-)}(\mathbf{q}_\perp) = \frac{iv^{2iv}}{2\pi}\int d\boldsymbol{\rho}\, \rho^{2iv}e^{i\mathbf{q}_\perp \cdot \boldsymbol{\rho}}\mathcal{A}'_{if}(\boldsymbol{\rho}), \quad (4)$$

respectively. Applying the inverse Fourier transform in Eq. (3) and replacing $\mathcal{A}'_{if}(\boldsymbol{\rho})$ in Eq. (4), results in

$$T_{fi}^{(-)}(\mathbf{q}_\perp) = \frac{iv^{2iv}}{(2\pi)^2}\int d\mathbf{q}'_\perp T_{fi}'^{(-)}(\mathbf{q}'_\perp)\int d\boldsymbol{\rho}\, \rho^{2iv}e^{i(\mathbf{q}_\perp - \mathbf{q}'_\perp)\cdot\boldsymbol{\rho}}. \quad (5)$$

The two-dimensional integral over the impact parameter can be done analytically to finally obtain [49,50]

$$T_{fi}^{(-)}(\mathbf{q}_\perp) = v \frac{iv^{2iv}(2\pi)^{-iv}}{2^4\pi^3}$$
$$\times \int d\mathbf{q}'_\perp T_{fi}'^{(-)}(\mathbf{q}'_\perp)|\mathbf{q}_\perp - \mathbf{q}'_\perp|^{-2(1+iv)}. \quad (6)$$

The last multidimensional integral in Eq. (6) is evaluated numerically using quadratures. As is well known, the eikonal approximation is valid as long as (i) the projectile suffers very small deflections in the collision (the so-called straight line approximation) and (ii) the velocity of the recoil ion remains small compared to that of the emitted electron. In the present work we only consider scattering angles of up to 0.5 mrad so that condition (i) is fulfilled. Additionally, because of the large recoil-ion to electron mass ratio, condition (ii) is satisfied as well.

In the computation of the transition amplitude $T_{fi}^{(-)}(\mathbf{q}_\perp)$, we use nonorthogonal Jacobi coordinates ($\mathbf{r}_P$, $\mathbf{r}_T$) to describe the ionization process [51]. These coordinates represent the position of the active electron with respect to the incoming projectile ($\mathbf{r}_P$) and the target ion ($\mathbf{r}_T$), respectively. $\mathbf{R}_T$ is also considered, representing the position of the heavy projectile with respect to the center of mass (CM) of the electron-target subsystem. If we neglect terms of orders $1/M_T$ and $1/M_P$, where M_T and M_P are the masses of the target ion nucleus and incident heavy ion, respectively, we can write $\mathbf{R}_T \approx \mathbf{r}_T - \mathbf{r}_P$. Within the prior CDW-EIS model, the transition amplitude can then be computed as

$$T_{fi}^{(-)}(\mathbf{q}_\perp) = \langle \chi_f^{-\text{CDW}} | W_i | \chi_i^{+\text{EIS}} \rangle, \quad (7)$$

where the initial (final) state distorted wave χ_i^+ (χ_f^-) is an approximation to the initial (final) state satisfying outgoing-wave (+) (incoming-wave (−)) asymptotic conditions. For the initial state the asymptotic form of the Coulomb distortion, the so-called eikonal phase, is used in the electron-projectile interaction together with a semianalytical Rothan-Hartree-Fock description for the initial bound-state wave function [52]:

$$\chi_i^{+\text{EIS}} = (2\pi)^{-3/2} \exp(i\mathbf{K}_i \cdot \mathbf{R}_T)\psi_{\text{RHF}}(\mathbf{r}_T)\mathcal{E}_v^+(\mathbf{r}_P), \quad (8)$$

where $\mathcal{E}_v^+(\mathbf{r}_P)$ is

$$\mathcal{E}_v^+(\mathbf{r}_P) = \exp\left[-i\frac{Z_P}{v}\ln(vr_P - \mathbf{v} \cdot \mathbf{r}_P)\right] \quad (9)$$

and $\psi_{\text{RHF}}(\mathbf{r}_T)$

$$\psi_{\text{RHF}}(\mathbf{r}_T) = \sum_{i=1}^5 N_i e^{-\zeta_i r_T}. \quad (10)$$

The normalization factors N_i and effective charges ζ_i are obtained from Ref. [52].

The final-state wave function is cast into the form

$$\chi_f^{-\text{CDW}} = (2\pi)^{-3/2} \exp(i\mathbf{K}_f \cdot \mathbf{R}_T)\chi_T^-(\mathbf{r}_T)C_{Pe}^-(\mathbf{r}_P), \quad (11)$$

where $C_{Pe}^-(\mathbf{r}_P)$ represents the Coulomb distortion of the ejected electron wave function due to the projectile, i.e.,

$$C_P^-(\mathbf{r}_P) = N(\nu_P) {}_1F_1(-i\nu_P, 1, -ik_P r_P - i\mathbf{k}_P \cdot \mathbf{r}_P). \quad (12)$$

$\nu_P = \frac{Z_P}{k_P}$ is the Sommerfeld parameter, $\mathbf{k}_P$ is the relative momentum of the electron-projectile subsystem, and $N(\nu_P)$ the Coulomb factor, defined as

$$N(\nu_P) = \Gamma(1 - i\nu_P)\exp(\pi\nu_P/2). \quad (13)$$

Additionally, the wave function of the ejected electron in the field of the target residual ion $\chi_T^-(\mathbf{r}_T)$ can be written as

$$\chi_T^-(\mathbf{r}_T) = (2\pi)^{-3/2}\exp(i\mathbf{k}_T \cdot \mathbf{r}_T)N(\nu_T)$$
$$\times {}_1F_1(-i\nu_T, 1, -ik_T r_T - i\mathbf{k}_T \cdot \mathbf{r}_T). \quad (14)$$

Here, $\nu_T = \frac{Z_{\text{eff}}}{k_T}$, $\mathbf{k}_T$ and Z_{eff} being the relative momentum and the effective charge of the electron-target subsystem, respectively, and $N(\nu_T)$ the Coulomb factor, defined now as

$$N(\nu_T) = \Gamma(1 - i\nu_T)\exp(\pi\nu_T/2). \quad (15)$$

We use a variational calculated $Z_{\text{eff}} = 1.6875$ for the final ion state, to partially account the influence of the remaining passive electron [53]. Small variations in the FDCS can be observed for other values of Z_{eff}. Finally, the perturbation potential W_i in Eq. (7) is defined by

$$(H_i - E_i)\chi_i^+ = W_i\chi_i^+, \quad (16)$$

where H_i is the full electronic initial Hamiltonian, neglecting the total CM motion. Particularly, W_i is composed of two differential operators [54], i.e.,

$$W_i = \frac{1}{2}\nabla_{\mathbf{r}_P}^2 - \nabla_{\mathbf{r}_P} \cdot \nabla_{\mathbf{r}_T}. \quad (17)$$

The details on extending the CDW-EIS approach to the H_2 molecule were reported in [55]. Here, we only summarize the main differences to the treatment of the He target. The molecular transition amplitude $T_{fi}^{(-)}(\mathbf{q}_\perp, \mathbf{R})$ can be written as

$$|T_{fi}^{(-)}(\mathbf{q}_\perp, \mathbf{R})|^2 = 2\{1 + \cos[\mathbf{p}_{\text{rec}} \cdot \mathbf{R}]\}|T_{fi}^{\text{eff},(-)}(\mathbf{q}_\perp)|^2, \quad (18)$$

where $\mathbf{p}_{\text{rec}} = \mathbf{q} - \mathbf{k}$ and $\mathbf{R}$ is the vector that identifies the relative position of the nuclei in the molecule.

In Eq. (18) $T_{fi}^{\text{eff},(-)}(\mathbf{q}_\perp)$ is the CDW-EIS transition amplitude corresponding to effective atomic centers located at the position of each H atom. The pure ionization of the H_2 molecule is modeled using an equilibrium distance $R = 1.4$ a.u. and the initial electronic state in each center is given by a hydrogenic function with a variational charge $Z = 1.19$ and the corresponding normalization factor $N_i(R) = 0.5459$. For the final electronic state, continuum wave functions centered on each target nucleus are used with an effective charge $Z_{\text{eff}} = \sqrt{2\varepsilon_i}$, being $\varepsilon_i = 0.566$ a.u. being the H_2 binding energy.

An average over all the molecular orientations should be performed in Eq. (18) for the case of randomly oriented molecules. Consequently, we obtain the molecular transition amplitude $T_{fi}^{(-)}(\mathbf{q}_\perp, \mathbf{R})$ as

$$|T_{fi}^{(-)}(\mathbf{q}_\perp, \mathbf{R})|^2 = 2\left\{1 + \frac{\sin\chi}{\chi}\right\}|T_{fi}^{\text{eff},(-)}(\mathbf{q}_\perp)|^2, \quad (19)$$

where $T_{fi}^{\text{eff},(-)}(\mathbf{q}_\perp)$ is the same atomic transition amplitude as in the case of oriented molecules and $\chi = p_{\text{rec}}R$. The H_2 FDCS can then be computed by inserting the molecular transition amplitude $T_{fi}^{(-)}(\mathbf{q}_\perp, \mathbf{R})$ [Eq (19)] in Eq. (1). The PT

interaction is included in the same way as in the case of the He atom. In both the He atom and H_2 molecule cases, when comparing with the experimental data, we use CDW-EIS-PT (CDW-EIS) to label the calculations with (without) the PT interaction included.

The 3DW-EIS is a fully quantum mechanical model which is described in Refs. [56,57], and here we provide only a short overview to show the similarities and differences with the CDW-EIS. Using the two-potential formulation, Foster *et al.* [56] showed that an exact transition matrix T_{fi} for Eq. (1) can be written as

$$T_{fi} = \langle \chi_f^- | V_i | \beta_i \rangle + \langle \chi_f^- | W_f^+ | \psi_i^+ - \beta_i \rangle, \qquad (20)$$

where χ_f^- is an approximate final-state wave function, W_f^+ is the final-state perturbation, ψ_i^+ is the exact initial-state wave function that must be approximated, and β_i is the asymptotic initial-state wave function, defined by

$$\beta_i = \phi_{PW}^+(\mathbf{K}_i, \mathbf{R}_T) \psi_t(\mathbf{r}_T), \qquad (21)$$

where $\phi_{PW}^+(\mathbf{K}_i, \mathbf{R}_T)$ is a plane wave for the incident proton and $\psi_t(\mathbf{r}_T)$ is the bound-state wave function for the target. For helium, this wave function is approximated as an analytical fit to the Hartree-Fock (HF) ground state wave function of helium [58] and, for the H_2 molecule, as the Dyson molecular orbital for the active electron $\psi_t(\mathbf{r}_T) = \phi_{1s}^{Dy}$ [59,60].

The final-state wave function χ_f^- is cast into the form

$$\chi_f^- = \phi_{PW}^-(\mathbf{K}_f, \mathbf{R}_T) C_{PT}^-(\mathbf{R}_T) \phi_{DW}^-(\mathbf{k}, \mathbf{r}_T) C_{Pe}^-(\mathbf{r}_P). \quad (22)$$

Here the factor $\phi_{PW}^-(\mathbf{K}_f, \mathbf{R}_T) C_{PT}^-(\mathbf{R}_T)$ is a Coulomb wave for the scattered proton in the field of the target ion which is composed of a plane wave times the Coulomb distortion factor $C_{PT}^-(\mathbf{R}_T)$ for a target charge of $+1$, $\phi_{DW}^-(\mathbf{k}, \mathbf{r}_T)$ is a distorted wave for the ejected electron in the field of the target, and $C_{Pe}^-(\mathbf{r}_P)$ is the Coulomb distortion factor for the interaction between the ejected electron and the proton. Compared to the final-state wave function for the CDW-EIS of Eq. (11), it is seen that the CDW-EIS approximates the final-state projectile wave function as a plane wave while the 3DW-EIS approximates this wave function as a Coulomb wave; the ejected electron wave function in the CDW is a Coulomb wave for an effective charge while it is a distorted wave in the 3DW; and the final-state ejected-electron-proton interaction is the same in both cases (with the exception of some approximations made in the CDW approach which should be valid for this case).

The exact scattering wave function ψ_i^+ in the entrance channel can be approximated by the eikonal initial state (EIS) introduced by Crothers and McCann [61], which is composed of the asymptotic initial-state wave function β_i times the eikonal phase which approximates the long range Coulomb initial-state interaction between the projectile and the target. We thus can write

$$\psi_i^+ \approx \beta_i \mathcal{E}_v^+(\mathbf{r}_P, \mathbf{R}_T), \qquad (23)$$

where $\mathcal{E}_v^+(\mathbf{r}_P, \mathbf{R}_T)$ is

$$\mathcal{E}_v^+(\mathbf{r}_P, \mathbf{R}_T) = \exp\left[i \frac{Z_p}{v} \ln\left(\frac{v R_T - \mathbf{v} \cdot \mathbf{R}_T}{v r_P - \mathbf{v} \cdot \mathbf{r}_P} \right) \right]. \qquad (24)$$

Comparing Eq. (23) with Eq. (8), it is seen that the CDW-EIS contains the asymptotic form of the proton-electron interaction only while the 3DW-EIS has this interaction plus the asymptotic form of the projectile-nucleus interaction as well. Different approximations are made for the initial bound state wave function as well, but this is probably not important.

In summary, the primary differences between the CDW-EIS and 3DW-EIS are (1) for the initial state, the CDW contains the asymptotic form of the initial state interaction between the projectile and target active electron while the 3DW has this interaction plus the asymptotic interaction with the target ion; (2) for the final state, the CDW approximates the final-state projectile wave function as a plane wave while the 3DW approximates this wave function as a Coulomb wave; and (3) for the final state, the ejected electron wave function in the CDW is a Coulomb wave while it is a distorted wave in the 3DW. From a numerical viewpoint, the biggest difference between the two calculations is the way in which the T matrix is evaluated. The CDW-EIS makes a straight-line approximation for the projectile which allows the integrals over the projectile coordinates to be evaluated analytically. The 3DW-EIS is a fully quantum mechanical calculation that makes no additional approximations, which means that a full six-dimensional (6D) integral over all projectile and electron coordinates must be performed for each fully differential cross section calculation. With the straight-line approximation made in the CDW-EIS, the PT interaction becomes an overall phase factor which can be factored out of the scattering amplitude, while in the 3DW-EIS this interaction is embedded in the 6D T-matrix integral and does not factor out of the integral.

IV. RESULTS AND DISCUSSION

In the θ_{el} dependence of the FDCS in the velocity-matching region, which we published previously, we observed a double peak structure for large θ_p [27]. The second peak, at larger E_{el}, known as the binary peak, occurs close to the direction of $\mathbf{q}$. Qualitatively, it can be viewed as a manifestation of first-order contributions, although, especially at small projectile velocities, higher-order contributions need to be considered for an accurate quantitative description. The first peak, located near $\theta_{el} = 0°$, to which we refer as the forward peak, is a manifestation of PCI and it is dominated by higher-order contributions. At small θ_p, $\mathbf{q}$ moves closer to $\theta_{el} = 0°$ and the FDCS are dominated by the forward peak. As a result, only a single peak near $\theta_{el} = 0°$ was observed. Since PCI is believed to maximize at the velocity matching, it was expected that the forward peak would be most pronounced at the cusp energy ($E_{el} = 40.8$ eV). Instead, for the He target it was found to keep increasing going from $E_{el} = 40.9$ to 37.9 eV (while for the H_2 target it maximized exactly at the cusp energy). However, it was not clear at which electron energy the forward peak maximizes because at that time no data were available between $E_{el} = 5.4$ and 37.9 eV. We therefore start our analysis of the new data by discussing the θ_{el} dependence of the FDCS for $E_{el} = 35.4$ eV.

These data are plotted in Fig. 1 for the He target as a function of θ_{el} for fixed θ_p of (from top to bottom) 0.1, 0.2, 0.3, and 0.5 mrad. Qualitatively, the data look very similar to those for $E_{el} = 37.9$ eV. Here, too, at large θ_p partly resolved forward
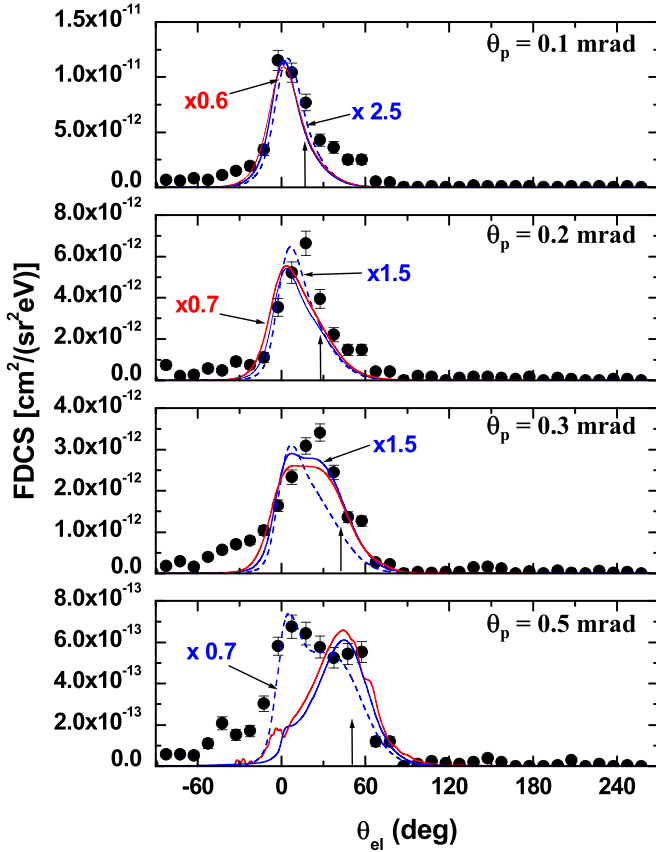
FIG. 1. Fully differential cross sections for electrons ejected from He into the scattering plane for an electron energy of 35.4 eV as a function of electron ejection angle. The projectile scattering angles are indicated in the insets of each panel. The dashed blue curves represent the CDW-EIS calculations, the solid blue curves the CDW-EIS-PT calculations, and the red curves the 3DW-EIS calculations.

FIG. 2. Same as Fig. 1, but the electron energy is fixed at 15.4 eV.

and binary peaks are visible and at the smallest θ_p the FDCS are dominated by the forward peak. Another similarity is that the ratio between the FDCS at $\theta_{el} = 0°$ and in the direction of **q** minimizes somewhere between $\theta_p = 0.2$ and 0.3 mrad, suggesting that the relative importance of PCI minimizes in this angular range. These θ_p correspond to a magnitude of **q** of about 1.4 to 1.6 a.u. A similar effect was observed earlier in the FDCS for ionization of He by fast heavy ion impact: there, a shift of the binary peak in the forward direction relative to **q**, caused by PCI, also minimized at similar q [32]. In contrast, for $E_{el} = 15.4$ eV the FDCS, shown for the same θ_p in Fig. 2, exhibit a rather different dependence on θ_{el}; here, the forward peak is completely absent, as expected, and the data maximize, except for $\theta_p = 0.5$ mrad, near the direction of **q**.

The comparison of the FDCS for $E_{el} = 15.4$, 35.4, and 37.9 eV demonstrates that PCI is much less prominent well below the velocity matching and that it plays a similarly important role for $E_{el} = 35.4$ and 37.9 eV. However, it does not provide quantitative information as to where exactly the FDCS for $\theta_{el} = 0°$ maximize. To address this question, in Fig. 3 we plot the FDCS for θ_{el} fixed at 0° as a function of E_{el} for fixed θ_p as indicated by the insets. In all cases, a very sharp peak structure, with a width of about 5 eV FWHM, is observed at around $E_{el} = 38$ eV, i.e., it is shifted relative to the
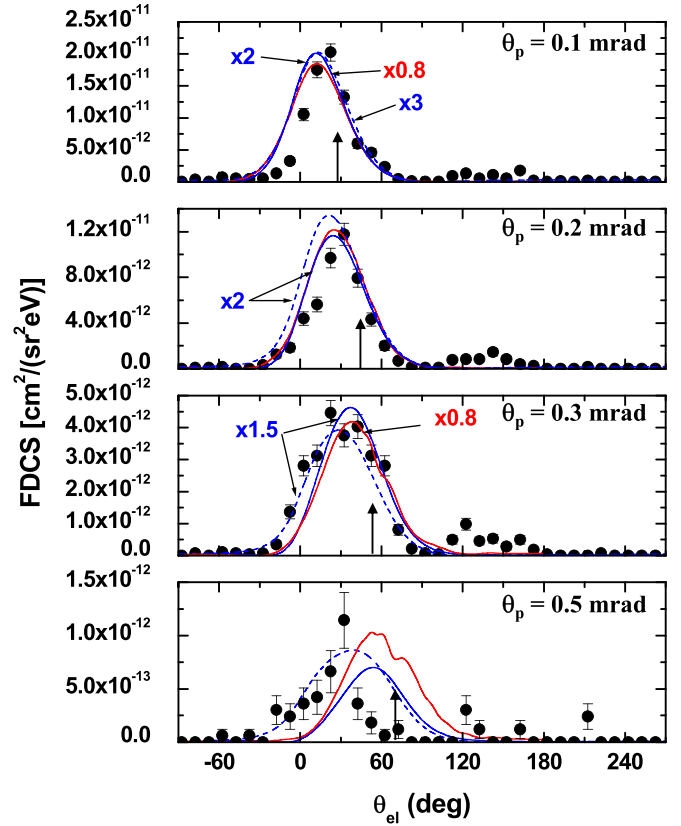
cusp energy by about 2 to 3 eV. A second, smaller and broader, maximum appears to be present near $E_{el} = 15$ eV. Although this is manifested by only one data point, it is nevertheless significant as it occurs systematically for all θ_p, except for 0.5 mrad, where no data are available for $E_{el} < 15$ eV.

The blue curves in Figs. 1–3 represent the continuum distorted-wave eikonal initial-state (CDW-EIS) calculations with (CDW-EIS-PT, solid curves) and without the PT interaction (CDW-EIS, dashed curves). The red curves show the three-body distorted-wave eikonal initial-state (3DW-EIS) calculations, which also account for the PT interaction. We emphasize that the 3DW-EIS and CDW-EIS-PT models are conceptually very similar and should essentially catch the same physics of the collision process.

The comparison between experiment and theory for the θ_{el} dependence of the FDCS at $E_{el} = 35.4$ eV is quite similar to what we reported previously for other electron energies in the velocity-matching regime: for the smallest θ_p all calculations reproduce the shape of the θ_{el} dependence very well. Only in magnitude are there some discrepancies in the CDW-EIS results and to a lesser extent in the 3DW-EIS results. However, with increasing θ_p the disagreement with the experimental data grows larger and the various theoretical models increasingly differ from each other. Surprisingly, the CDW-EIS calculation, which conceptually is the "least complete" model, yields by far the best agreement with the measured FDCS for $\theta_p = 0.5$ mrad. For $E_{el} = 15.4$ eV, on the other hand, in the shape of the θ_{el} dependence of the
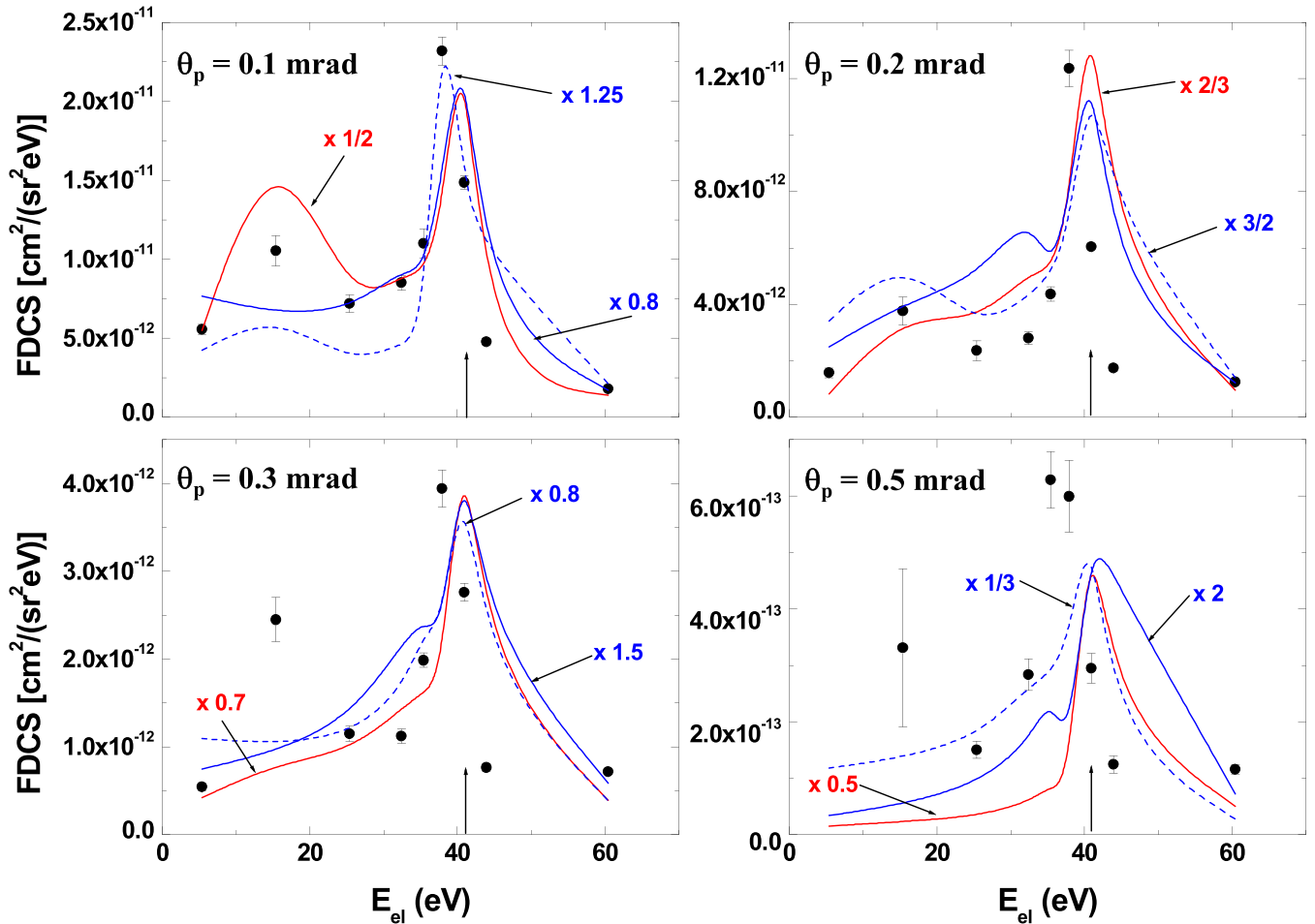
FIG. 3. Fully differential cross sections for electrons ejected from He in the forward direction ($\theta_{el} = 0°$) as a function of the electron energy. The projectile scattering angles are indicated in the insets of each panel. Curves: same as in Figs. 1 and 2.

FDCS the agreement between theory and experiment is satisfactory up to $\theta_p = 0.3$ mrad. Furthermore, for these θ_p the 3DW-EIS model even reproduces the magnitude of the measured FDCS within less than 20%. In contrast, the agreement of all calculations with the data at $\theta_p = 0.5$ mrad is rather poor. Here again, the CDW-EIS model gives overall significantly better results than the calculations including the PT interaction. This comparison between theory and experiment near the matching velocity ($E_{el} = 35.4$ eV) and well below the matching velocity ($E_{el} = 15.4$ eV) reinforces our earlier conclusion that kinematic regions, for which PCI is very strong, are outside the regime of validity of distorted-wave approaches.

In the energy dependence of the FDCS for θ_{el} fixed at $0°$, shown in Fig. 3, the agreement between experiment and theory is mixed. All calculations reproduce a very sharp cusp peak in the velocity-matching regime. However, both calculations including the PT interaction do not reproduce the shift of the centroid of 2 to 3 eV to smaller energies seen in the data. On the other hand, the CDW-EIS model reproduces the cusp peak in the experimental data at $\theta_p = 0.1$ mrad almost perfectly. At $\theta_p = 0.5$ mrad, the cusp peak in this calculation is also shifted, but only by 1 eV. At the other two scattering angles the CDW-EIS results exhibit a similar shape and location of the cusp peak as the calculations including the PT

interaction. At present, we cannot offer any explanation for this shift observed in the data and in the CDW-EIS calculations.

The smaller peak structure seen in the experimental data at about 15 eV is qualitatively reproduced by the CDW-EIS and the 3DW-EIS calculations. However, the former model underestimates its height (relative to the cusp peak) and the latter overestimates it for $\theta_p = 0.1$ mrad, while these trends are reversed for $\theta_p = 0.2$ mrad. Interestingly, in the CDW-EIS approach this maximum is completely removed by the inclusion of the PT interaction. An additional structure is seen in the CDW-EIS-PT calculation at about $E_{el} = 30$ eV at all θ_p, except for 0.1 mrad, which is present neither in the experimental data nor in the other two calculations.

It should be noted that fixing θ_{el} at $0°$ in the energy dependence of the FDCS is about as selective on a strong role of PCI as fixing E_{el} near the cusp energy in the angular dependence of the FDCS. Indeed, in the energy dependence for $\theta_{el} = 0°$ the discrepancies between theory and experiment are similarly severe as in the angular dependence of the FDCS, especially at large θ_p. In addition, conceptually very similar theoretical models yield qualitatively different results. Once again, these observations reinforce our earlier conclusion [27] that kinematic regimes for which PCI plays an important role are particularly challenging to distorted
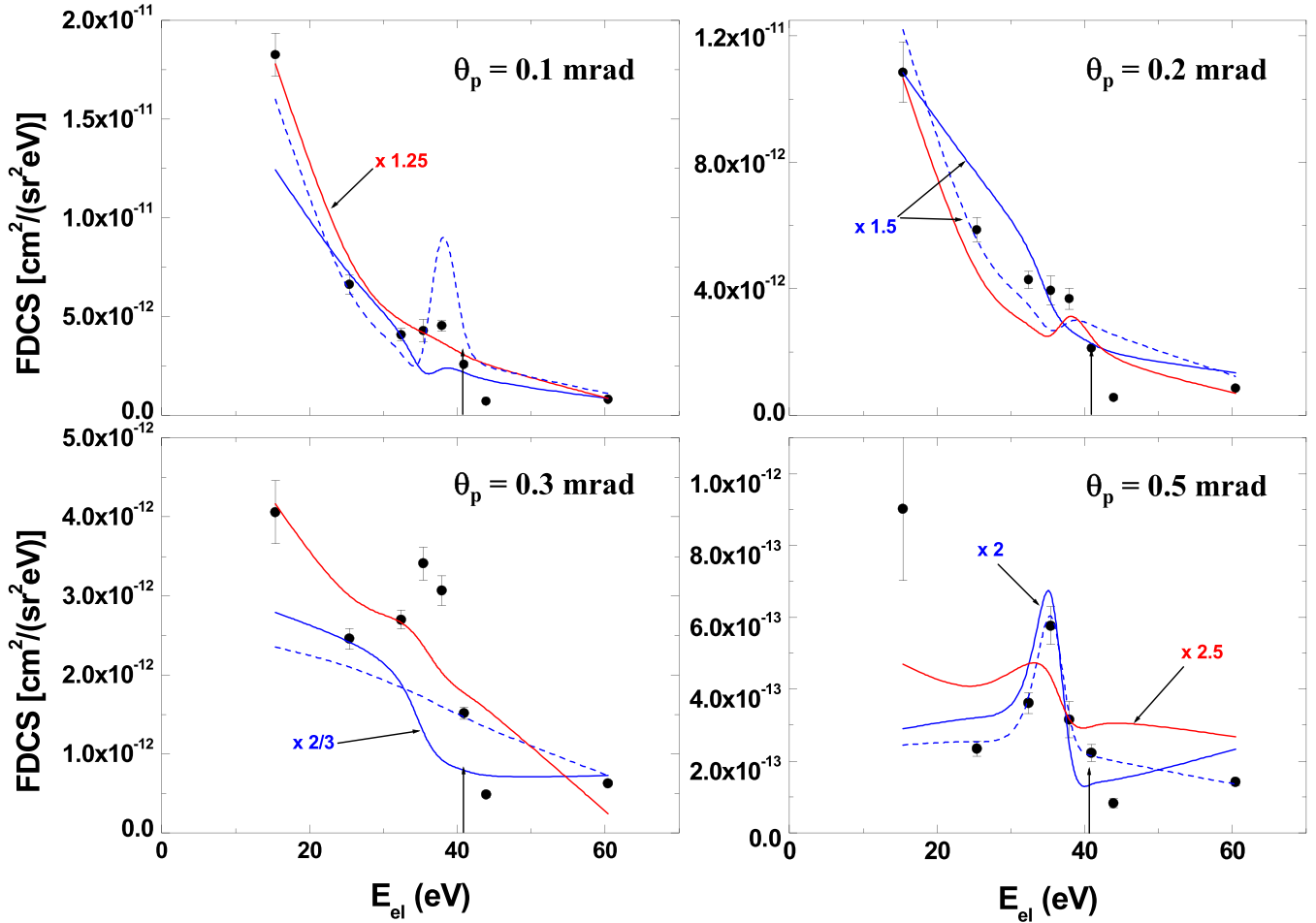
FIG. 4. Fully differential cross sections for electrons ejected from He into the scattering plane at a fixed ejection angle of $\theta_{el} = 30°$ as a function of the electron energy. The projectile scattering angles are indicated in the insets of each panel. Curves: same as solid curves in Figs. 1–3.

wave approaches. One might expect the agreement between experiment and theory to be significantly improved in the energy dependence of the FDCS for θ_{el} fixed at a value closer to the direction of **q**. This is closer to the region of the binary peak and one might expect PCI effects to be rather insignificant.

In Fig. 4, such data are shown for $\theta_{el} = 30°$ for the same θ_p as in Fig. 3. For $\theta_p = 0.1$ and 0.2 mrad, indeed the cusp peak has nearly completely disappeared, signifying a strongly reduced role of PCI. Furthermore, the agreement between theory and experiment at $\theta_p = 0.1$ mrad is significantly improved compared to $\theta_{el} = 0°$ and the various calculations do not differ as much from each other, at least up to the cusp peak region. However, for $\theta_p > 0.2$ mrad, an increasingly pronounced cusp peak emerges, which shows that there the FDCS are substantially affected by PCI. At first glance, this may look like a surprising observation because in double differential energy spectra (i.e., FDCS integrated over all projectile solid angles) the cusp peak tends to disappear rapidly for θ_{el} larger than just a few degrees (e.g., [62–64]). However, it should be noted that the presence of a cusp peak at large θ_p in the data of Fig. 4 is not in conflict with the double differential electron spectra. The integral of the FDCS over the projectile solid angle is dominated by θ_p smaller than 0.2 mrad so that the

cusp peak observed at larger θ_p is not visible in the double differential cross sections (DDCS). On the other hand, even if the DDCS are further integrated over all electron solid angles, a weak "shoulder structure" near the cusp energy, of similar shape to that seen in Fig. 4 for $\theta_p = 0.1$ and 0.2 mrad, is found in the resulting single differential energy-loss spectrum (see also [65]). Furthermore, strong PCI effects for θ_{el} significantly larger than 0° are also routinely observed for fast highly charged ion impact, where they manifest themselves by a forward shift of the binary peak relative to **q** (see, e.g., [28,29,32]).

The experimental data of Fig. 4 are to some extent qualitatively reproduced by theory insofar as in some cases the calculations also exhibit a cusp peak. Furthermore, the 3DW-EIS model correctly predicts that the cusp peak becomes increasingly pronounced with increasing θ_p. However, the height of the cusp peak is systematically underestimated. In contrast, the CDW-EIS-PT model only shows a clear cusp peak at $\theta_p = 0.5$ mrad and generally tends to be in worse agreement with the data than the 3DW-EIS results. Furthermore, the inclusion of the PT interaction in this model does not lead to a systematic improvement in the agreement with the data. In fact, the shape of the cusp peak at $\theta_p = 0.5$ mrad is better reproduced by the CDW-EIS model.
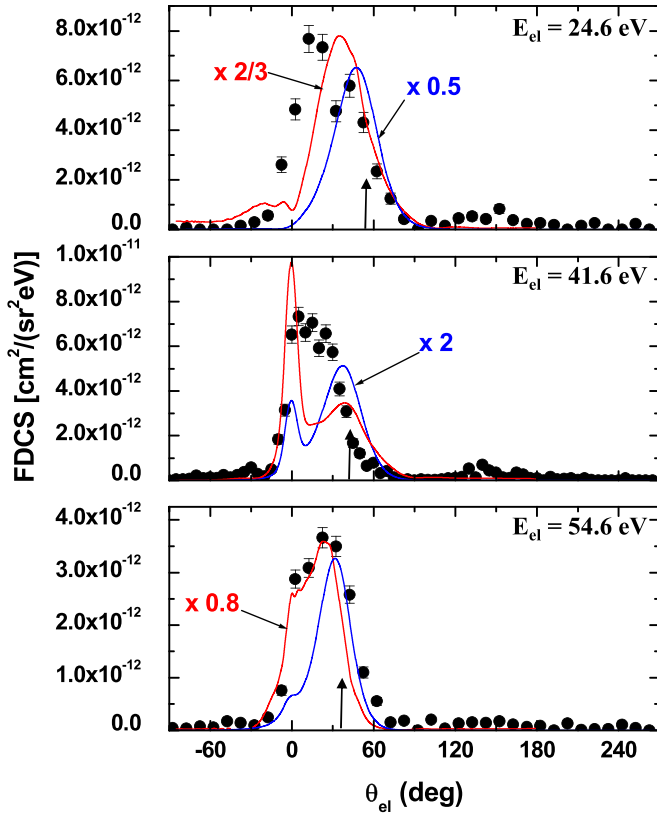
FIG. 5. Fully differential cross sections for electrons ejected from H_2 into the scattering plane for a fixed projectile scattering angle of 0.325 mrad and for electron energies as indicated in the insets, as a function of electron ejection angle. Curves: same as in Fig. 4.
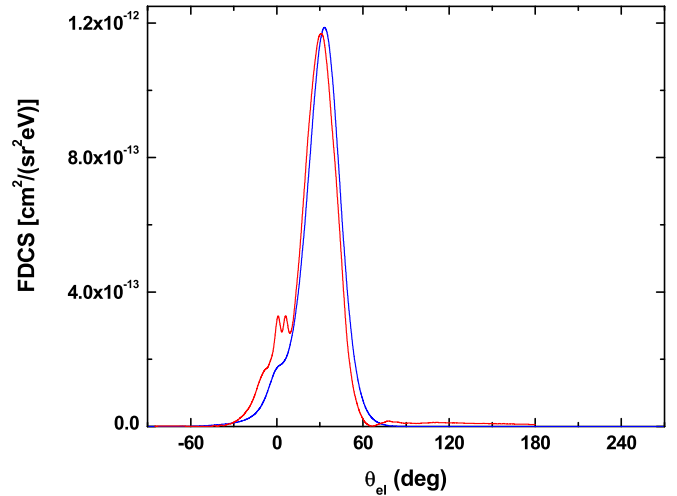

FIG. 6. Calculated fully differential cross sections for electrons ejected from atomic H into the scattering plane for a fixed projectile scattering angle of 0.325 mrad and electron energy of 54.6 eV as a function of electron ejection angle. Curves: same as in Fig. 4.

Furthermore, this latter calculation shows a rather pronounced cusp peak at $\theta_p = 0.1$ mrad, while in the CDW-EIS-PT results a small minimum is seen near the cusp energy. Two different interaction sequences (in a classical description) have been identified as mostly contributing to PCI [26,27,66,67]. Both start with the primary projectile-electron interaction, lifting the electron to the continuum, and both end with a second projectile-electron interaction, leading to both particles attracting each other towards the projectile beam axis. In between, either the electron (V_{ep}-V_{et}-V_{ep} sequence) or the projectile (V_{ep}-V_{pt}-V_{ep} sequence) is redirected by an interaction with the residual-target ion. The pronounced cusp peak in the CDW-EIS calculation at $\theta_p = 0.1$ mrad shows that the V_{ep}-V_{et}-V_{ep} sequence plays an important role in PCI at small θ_p. However, the fact that the inclusion of the PT interaction in this model results in a minimum strongly suggests that the other sequence is very important as well. The minimum can probably only be explained by destructive interference (e.g., between both sequences). The absence of a minimum in the experimental data suggests that the V_{ep}-V_{pt}-V_{ep} sequence is overestimated in the CDW-EIS-PT approach. Better agreement with the data in the cusp region is achieved with the 3DW-EIS model.

The behavior of the CDW-EIS calculations, with or without PT interaction, is somewhat erratic. For example, going from $\theta_p = 0.3$ to 0.5 mrad the energy dependence of the FDCS in

the cusp region rapidly changes from a smooth decline (CDW-EIS) or a step (CDW-EIS-PT) to a pronounced peak structure. This is consistent with the presence of strong interference effects, which tend to be quite sensitive to kinematic parameters, such as the scattering angle, determining the phase angle. It is also consistent with the sensitivity of the FDCS to the projectile coherence length found in theoretical calculations [43].

The important observations in the measured FDCS for ionization of He and in the comparison with theory can be summarized as follows: first, there are large discrepancies between experiment and theory and large differences between conceptually very similar models under kinematic conditions where PCI plays an important role. Second, the inclusion of the PT interaction does not lead to significant overall improved agreement with the measured data. In fact, for several kinematic settings the best agreement is achieved with the model not including the PT interaction. Third, PCI can be rather strong at relatively large electron ejection angles. Finally, in some cases the theoretical calculations exhibit a somewhat erratic behavior, which we take as an indication for strong interference effects.

In Fig. 5 we compare the angular dependence of the FDCS for ionization of H_2 for an electron energy below the velocity match (top panel, $E_{el} = 14.6$ eV or $v_{el}/v_p = 0.77$), nearly at the velocity match (center panel, $E_{el} = 41.6$ eV or $v_{el}/v_p = 1.01$), and above the velocity match (bottom panel, $E_{el} = 54.6$ eV or $v_{el}/v_p = 1.16$). In all cases, θ_p is fixed at 0.325 mrad. The curves represent the same calculations as in Figs. 1–4. Like for the He target, here too, the discrepancies between experiment and theory and between the theoretical models are particularly large at the cusp energy. However, one important difference is that for H_2 even well outside the velocity-matching regime the discrepancies between the CDW-EIS-PT calculations and the experimental data are quite severe. The 3DW-EIS approach yields significantly better agreement in this kinematic region, but it is nevertheless somewhat worse than for He.
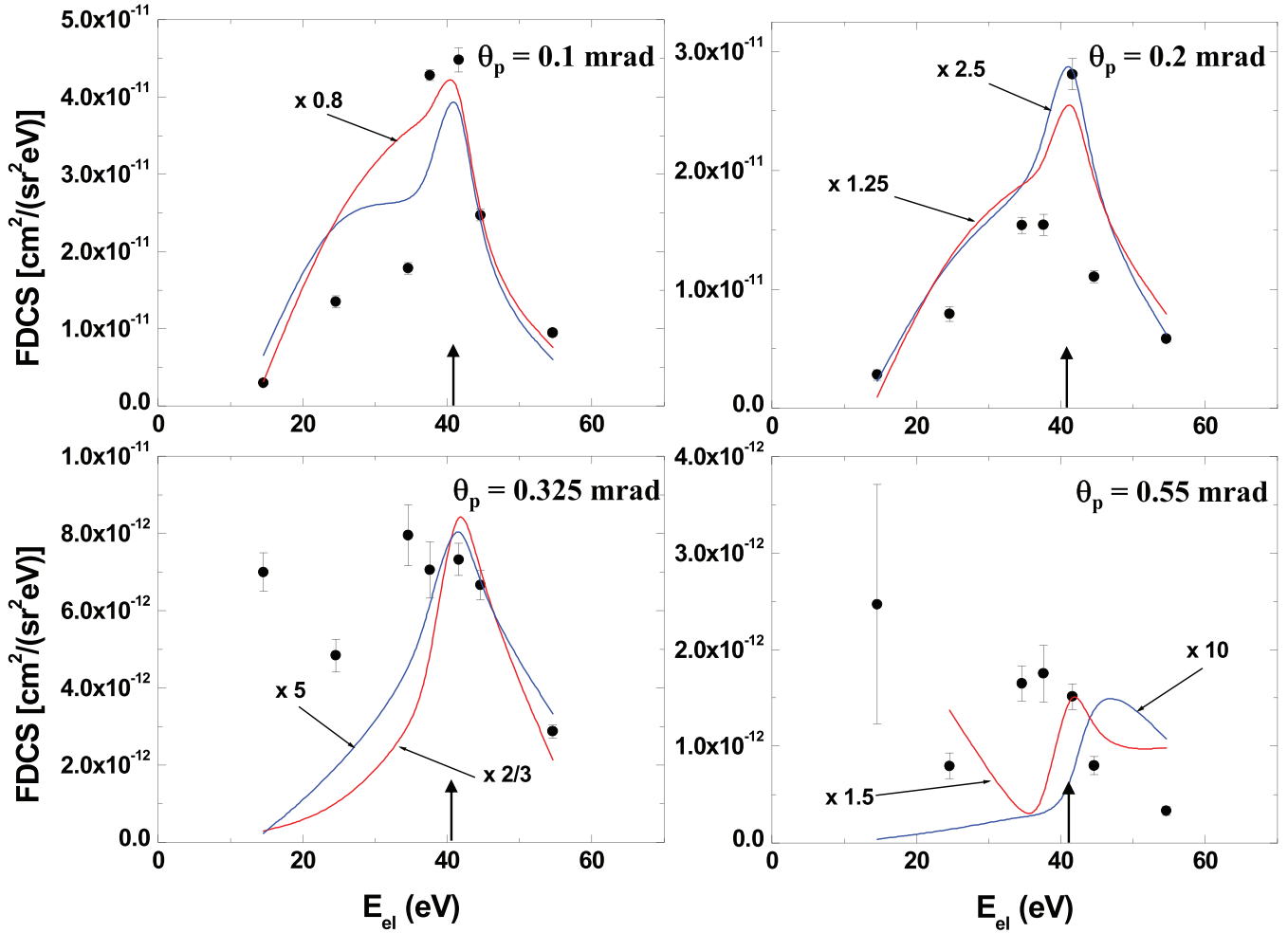
FIG. 7. Same as Fig. 3, but for electron ejection from H_2.

One important difference between H_2 and He is the presence of molecular two-center interference for the former target [68]. The description of this interference probably represents the largest difference between the CDW-EIS-PT and 3DW-EIS models. In the former, it is accounted for in an *ad hoc* manner by multiplying the FDCS for ionization of atomic H with a model interference factor of the form $f = 1 + \sin(p_{rec}R)/(p_{rec}R)$, where p_{rec} is the recoil-ion momentum and R is the internuclear distance of the molecule at equilibrium (see Sec. III for more details). In the latter model, in contrast, the interference is included from first principles in the transition amplitude. In the case of electron impact the interference pattern calculated with the 3DW-EIS model was found to be phase shifted by π relative to the model interference term [69]. This could explain the large differences between the 3DW-EIS and CDW-EIS-PT calculations even well outside the velocity-matching regime. Indeed, for ionization of atomic hydrogen, which is not afflicted with molecular two-center interference, both calculations, shown for $E_{el} = 54.6$ eV and $\theta_p = 0.325$ mrad in Fig. 6, give similar results.

In Fig. 7 the ejected-electron-energy dependence of the FDCS for H_2 is shown for $\theta_{el} = 0°$ and for the scattering angles as indicated in the insets. As for the He target, here too a sharp cusp peak is found for $\theta_p = 0.1$ and 0.2 mrad.

However, in contrast to He, the cusp peak is not shifted relative to the energy corresponding to the velocity match. Previously published data only covered electron energies close to the cusp energy and 14.6 eV [27]. For these energies the FDCS seemed to exhibit a rather flat behavior for $\theta_p = 0.325$ and 0.55 mrad. With the new data points there actually appears to be a maximum for the two larger θ_p as well, although it is significantly broader than at small θ_p.

Regarding the comparison between theory and experiment, an important advantage of analyzing the energy dependence of the FDCS is that the molecular two-center interference term hardly varies at all over the energy range plotted in Fig. 7. Therefore, if the differences between the CDW-EIS-PT and 3DW-EIS calculations of the angular dependence were mostly due to the different treatment of this interference then both models should yield results that are more similar in the energy dependence. Indeed, for $\theta_p = 0.325$ mrad, for which the angular dependence of the FDCS is plotted in Fig. 5, both calculations are much closer to each other in shape, although there are large differences in magnitude. In contrast, large and qualitative differences are visible at $\theta_p = 0.55$ mrad, illustrating that, in spite of their conceptual similarity, both models significantly depart from each other in the description of the few-body dynamics beyond molecular two-center interference.

V. CONCLUSIONS

We extended previous measurements of fully differential cross sections on ionization of He and H_2 by 75 keV proton impact in the region of the ejected electron-projectile velocity matching to a broad energy range covering electron-to-projectile speed ratios from 0.36 to 1.22. The data were compared to various conceptually similar distorted-wave calculations, with and without inclusion of the interaction between projectile and residual target ion (PT interaction). For the He target, qualitatively good agreement between experiment and theory is found for relatively small projectile scattering angles and ejected electron energies well outside the velocity-matching regime. However, with increasing scattering angle and approaching the velocity matching, increasing discrepancies between experiment and theory are observed. At the same time, the various calculations increasingly depart from each other. Especially at the largest scattering angle (0.5 mrad) the experimental data and the various calculations do not even resemble each other qualitatively. Another important observation is that the overall agreement between experiment and theory is not improved with the inclusion of the PT interaction. In fact, in some cases significantly better agreement is obtained using the calculation without the PT interaction.

Higher-order mechanisms including the post-collision interaction (PCI) are known to be particularly important near the velocity-matching regime. Therefore, the severe discrepancies between the data and the various calculations in this region demonstrate that kinematic conditions for which PCI is strong fall outside the regime of validity of distorted-wave models. The observation that the inclusion of the PT interaction does not lead to overall improved agreement suggests that higher-order mechanisms leading to PCI which include this interaction represent a particularly large challenge to theory. However, this does not necessarily mean that such mechanisms are generally underestimated. Features

characteristic of PCI could also be suppressed through destructive interference even if the role of the PT interaction is overestimated.

In the case of the H_2 target discrepancies between experiment and theory and differences between the calculations are already quite significant well outside the velocity-matching regime and at small scattering angles. Here, in addition to the difficulties in accurately describing the few-body dynamics under kinematic conditions were PCI is strong, another challenge is represented by molecular two-center interference. The description of this interference represents the largest difference between the CDW-EIS and 3DW-EIS approaches. For electron impact, it was shown already that this difference can result in a phase shift in the interference pattern calculated with both methods. It would thus not be surprising if for proton impact the FDCS calculated with the same approaches were also afflicted by large differences in the two-center interference term.

[1] M. Schulz, R. Moshammer, D. Fischer, H. Kollmus, D. Madison, S. Jones, and J. Ullrich, Nature (London) **422**, 48 (2003).

[2] T. N. Rescigno, M. Baertschy, W. Isaacs, and C. McCurdy, Science **286**, 2474 (1999).

[3] H. Ehrhardt, K. Jung, G. Knoth, and P. Schlemmer, Z. Phys. D **1**, 3 (1986).

[4] A. Lahman-Bennani, J. Phys. B **24**, 2401 (1991).

[5] R. Dörner, V. Mergel, O. Jagutzski, L. Spielberger, J. Ullrich, R. Moshammer, and H. Schmidt-Böcking, Phys. Rep. **330**, 95 (2000).

[6] J. Ullrich, R. Moshammer, A. Dorn, R. Dörner, L. Schmidt, and H. Schmidt-Böcking, Rep. Prog. Phys. **66**, 1463 (2003).

[7] M. Schulz and D. Madison, Int. J. Mod. Phys. A **21**, 3649 (2006).

[8] H. Ehrhardt, M. Schulz, T. Tekaat, and K. Willmann, Phys. Rev. Lett. **22**, 89 (1969).

[9] G. Stefani, L. Avaldi, and R. Camilloni, J. Phys. B **23**, L227 (1990).

[10] A. Murray, M. Woolf, and F. Read, J. Phys. B **25**, 3021 (1992).

[11] J. Röder, H. Ehrhardt, I. Bray, D. Fursa, and I. McCarthy, J. Phys. B **29**, 2103 (1996).

[12] R. W. van Boeyen, N. Watanabe, J. W. Cooper, J. P. Doering, J. H. Moore, and M. A. Coplan, Phys. Rev. A **73**, 032703 (2006).

[13] M. Dürr, C. Dimopoulou, B. Najjari, A. Dorn, K. Bartschat, I. Bray, D. V. Fursa, Z. Chen, D. H. Madison, and J. Ullrich, Phys. Rev. A **77**, 032717 (2008).

[14] X. Ren, A. Senftleben, T. Pflüger, A. Dorn, J. Colgan, M. S. Pindzola, O. Al-Hagan, D. H. Madison, I. Bray, D. V. Fursa, and J. Ullrich, Phys. Rev. A **82**, 032712 (2010).

[15] E. S. Casagrande, A. Naja, F. Mezdari, A. Lahman-Bennani, P. Bolognesi, B. Joulakian, O. Chuluunbaatar, O. Al-Hagan, D. Madison, D. Fursa, and I. Bray, J. Phys. B **41**, 025204 (2008).

[16] S. M. Bellm, C. J. Colyer, B. Lohmann, and C. Champion, Phys. Rev. A **85**, 022710 (2012).

[17] B. A. de Harak, K. Bartschat, and N. L. S. Martin, Phys. Rev. Lett. **100**, 063201 (2008).

[18] J. Williams, P. Bartlett, and A. Stelbovics, Phys. Rev. Lett. **96**, 123201 (2006).

[19] X. Ren, A. Senftleben, T. Pflüger, K. Bartschat, O. Zatsarinny, J. Berakdar, J. Colgan, M. Pindzola, I. Bray, D. V. Fursa, and A. Dorn, Phys. Rev. A **92**, 052707 (2015).

[20] I. Bray and D. V. Fursa, Phys. Rev. A **54**, 2991 (1996).

[21] J. Colgan, M. S. Pindzola, G. Childers, and M. A. Khakoo, Phys. Rev. A **73**, 042710 (2006).

[22] A. T. Stelbovics, I. Bray, D. V. Fursa, and K. Bartschat, Phys. Rev. A **71**, 052716 (2005).

[23] N. V. Maydanyuk, A. Hasan, M. Foster, B. Tooke, E. Nanni, D. H. Madison, and M. Schulz, Phys. Rev. Lett. **94**, 243201 (2005).

[24] S. Sharma, T. P. Arthanayaka, A. Hasan, B. R. Lamichhane, J. Remolina, A. Smith, and M. Schulz, Phys. Rev. A **90**, 052710 (2014).

[25] A. Hasan, S. Sharma, T. Arthanayaka, B. Lamichhane, J. Remolina, S. Akula, D. Madison, and M. Schulz, J. Phys. B **47**, 215201 (2014).

[26] M. Dhital, S. Bastola, A. Silvus, A. Hasan, B. R. Lamichhane, E. Ali, M. F. Ciappina, R. A. Lomsadze, D. Cikota, B. Boggs, D. H. Madison, and M. Schulz, Phys. Rev. A **99**, 062710 (2019).

[27] M. Dhital, S. Bastola, A. Silvus, B. R. Lamichhane, E. Ali, M. F. Ciappina, R. Lomsadze, A. Hasan, D. H. Madison, and M. Schulz, Phys. Rev. A **100**, 032707 (2019).

[28] M. Schulz, R. Moshammer, A. Perumal, and J. Ullrich, J. Phys. B **35**, L161 (2002).

[29] D. Fischer, R. Moshammer, M. Schulz, A. Voitkiv, and J. Ullrich, J. Phys. B **36**, 3555 (2003).

[30] M. Schulz, R. Moshammer, A. Voitkiv, B. Najjari, and J. Ullrich, Nucl. Instrum. Methods B **235**, 296 (2005).

[31] R. Hubele, A. LaForge, M. Schulz, J. Goullon, X. Wang, B. Najjari, N. Ferreira, M. Grieser, V. L. B. de Jesus, R. Moshammer, K. Schneider, A. B. Voitkiv, and D. Fischer, Phys. Rev. Lett. **110**, 133201 (2013).

[32] M. Schulz, B. Najjari, A. B. Voitkiv, K. Schneider, X. Wang, A. C. Laforge, R. Hubele, J. Goullon, N. Ferreira, A. Kelkar, M. Grieser, R. Moshammer, J. Ullrich, and D. Fischer, Phys. Rev. A **88**, 022704 (2013).

[33] K. Schneider, M. Schulz, X. Wang, A. Kelkar, M. Grieser, C. Krantz, J. Ullrich, R. Moshammer, and D. Fischer, Phys. Rev. Lett. **110**, 113201 (2013).

[34] H. Gassert, O. Chuluunbaatar, M. Waitz, F. Trinter, H.-K. Kim, T. Bauer, A. Laucke, C. Müller, J. Voigtsberger, M. Weller, J. Rist, M. Pitzer, S. Zeller, T. Jahnke, L. P. H. Schmidt, J. Williams, S. A. Zaytsev, A. A. Bulychev, K. A. Kouzakov, H. Schmidt-Böcking, R. Dörner, Y. V. Popov, and M. S. Schöffler, Phys. Rev. Lett. **116**, 073201 (2016).

[35] O. Chuluunbaatar, K. A. Kouzakov, S. A. Zaytsev, A. S. Zaytsev, V. L. Shablov, Y. V. Popov, H. Gassert, M. Waitz, H.-K. Kim, T. Bauer, A. Laucke, C. Müller, J. Voigtsberger, M. Weller, J. Rist, K. Pahl, M. Honig, M. Pitzer, S. Zeller, T. Jahnke, L. P. H. Schmidt, H. Schmidt-Böcking, R. Dörner, and M. S. Schöffler, Phys. Rev. A **99**, 062711 (2019).

[36] H. R. J. Walters and C. T. Whelan, Phys. Rev. A **92**, 062712 (2015).

[37] M. McGovern, D. Assafrão, J. R. Mohallem, C. T. Whelan, and H. R. J. Walters, Phys. Rev. A **81**, 042704 (2010).

[38] I. B. Abdurakhmanov, A. S. Kadyrov, S. U. Alladustov, I. Bray, and K. Bartschat, Phys. Rev. A **100**, 062708 (2019).

[39] M. F. Ciappina, M. S. Pindzola, and J. Colgan, Phys. Rev. A **87**, 042706 (2013).

[40] M. Schulz, in *Advances in Atomic, Molecular, and Optical Physics*, edited by E. Arimondo, C. Lin, and S. Yelin, Vol. 66 (Elsevier, Amsterdam, 2017), p. 508.

[41] K. N. Egodapitiya, S. Sharma, A. Hasan, A. C. Laforge, D. H. Madison, R. Moshammer, and M. Schulz, Phys. Rev. Lett. **106**, 153202 (2011).

[42] T. Arthanayaka, S. Sharma, B. Lamichhane, A. Hasan, J. Remolina, S. Gurung, and M. Schulz, J. Phys. B **48**, 071001 (2015).

[43] L. Nagy, F. Járai-Szabó, S. Borbély, T. Arthanayaka, B. Lamichhane, A. Hasan, and M. Schulz, in *The State-of-The-Art-Reviews on Energetic Ion-Atom and Ion-Molecule Collisions*, edited by D. Belkić, I. Bray, and A. Kadyrov, Vol. 2 (World Scientific, Singapore, 2019) p. 129.

[44] A. Gaus, W. T. Htwe, J. Brand, T. Gay, and M. Schulz, Rev. Sci. Instrum. **65**, 3739 (1994).

[45] M. Schulz, T. Vajnai, A. D. Gaus, W. Htwe, D. H. Madison, and R. E. Olson, Phys. Rev. A **54**, 2951 (1996).

[46] J. S. Alexander, A. C. Laforge, A. Hasan, Z. S. Machavariani, M. F. Ciappina, R. D. Rivarola, D. H. Madison, and M. Schulz, Phys. Rev. A **78**, 060701(R) (2008).

[47] M. F. Ciappina, O. A. Fojón, and R. D. Rivarola, J. Phys. B **47**, 042001 (2014).

[48] P. D. Fainstein, V. H. Ponce, and R. D. Rivarola, J. Phys. B **24**, 3091 (1991).

[49] G. Gasaneo, W. Cravero, M. D. Sánchez, and C. R. Garibotti, Phys. Rev. A **54**, 439 (1996).

[50] M. D. Sánchez, W. R. Cravero, and C. R. Garibotti, Phys. Rev. A **61**, 062709 (2000).

[51] N. Stolterfoht, R. D. DuBois, and R. D. Rivarola, *Electron Emission in Heavy Ion-Atom Collisions* (Springer, Berlin, 1997).

[52] E. Clemente and C. Roetti, At. Data Nucl. Data Tables **14**, 177 (1974).

[53] B. H. Brandsen and C. J. Joachain, *Physics of Atoms and Molecules* (John Wiley & Sons, New York, 1990).

[54] D. S. F. Crothers and L. J. Dubé, Adv. At. Mol. Opt. Phys. **30**, 287 (1992).

[55] M. E. Galassi, R. D. Rivarola, P. D. Fainstein, and N. Stolterfoht, Phys. Rev. A **66**, 052705 (2002).

[56] M. Foster, D. H. Madison, J. L. Peacher, and J. Ullrich, J. Phys. B **37**, 3797 (2004).

[57] M. Foster, D. H. Madison, J. L. Peacher, M. Schulz, S. Jones, D. Fischer, R. Moshammer, and J. Ullrich, J. Phys. B **37**, 1565 (2004).

[58] F. W. Byron and C. J. Joachain, Phys. Rev **146**, 1 (1966).

[59] J. Gao, D. H. Madison, and J. L. Peacher, J. Phys. B **39**, 1275 (2006).

[60] U. Chowdhury, M. Schulz, and D. H. Madison, Phys. Rev. A **83**, 032712 (2011).

[61] D. S. F. Crothers and J. F. McCann, J. Phys. B **16**, 3229 (1983).

[62] G. Bernardi, P. Focke, and W. Meckbach, Phys. Rev. A **55**, R3983 (1997).

[63] L. Sarkadi, U. Brinkmann, A. Báder, R. Hippler, K. Tökési, and L. Gulyás, Phys. Rev. A **58**, 296 (1998).

[64] D. R. Schultz and C. O. Reinhold, Phys. Rev. A **50**, 2390 (1994).

[65] J. Park and F. D. Schowengerdt, Phys. Rev. **185**, 152 (1969).

[66] L. Sarkadi, L. Gulyás, and L. Lugosi, Phys. Rev. A **65**, 052715 (2002).

[67] M. Schulz, A. C. Laforge, K. N. Egodapitiya, J. S. Alexander, A. Hasan, M. F. Ciappina, A. C. Roy, R. Dey, A. Samolov, and A. L. Godunov, Phys. Rev. A **81**, 052705 (2010).

[68] N. Stolterfoht, B. Sulik, V. Hoffmann, B. Skogvall, J. Y. Chesnel, J. Ragnama, F. Frèmont, D. Hennecart, A. Cassimi, X. Husson, A. L. Landers, J. A. Tanis, M. E. Galassi, and R. D. Rivarola, Phys. Rev. Lett. **87**, 023201 (2001).

[69] A. Senftleben, T. Pflüger, X. Ren, O. Al-Hagan, B. Najjari, D. Madison, A. Dorn, and J. Ullrich, J. Phys. B **43**, 081002 (2010).